

Salih K. Kalyoncu

The Scientific and Technological
Research Council of Turkey,
Gebze 41400, Turkey;
EECS Department,
University of California,
Irvine, CA 92697
e-mail: skalyonc@uci.edu

Rasul Torun

EECS Department,
University of California,
Irvine, CA 92697;
EECS Department,
Istanbul Sehir University,
Istanbul 34662, Turkey
e-mail: rtorun@uci.edu

Yuewang Huang

EECS Department,
University of California,
Irvine, CA 92697
e-mail: yuewangh@uci.edu

Qiancheng Zhao

EECS Department,
University of California,
Irvine, CA 92697
e-mail: qianchez@uci.edu

Ozdal Boyraz

EECS Department,
University of California,
Irvine, CA 92697;
EECS Department,
Istanbul Sehir University,
Istanbul 34662, Turkey
e-mail: oboyraz@uci.edu

Fast Dispersive Laser Scanner by Using Digital Micro Mirror Arrays

We demonstrate a fast dispersive laser scanning system by using MEMS digital micro-mirror arrays technology. The proposed technique utilizes real-time dispersive imaging system, which captures spectrally encoded images with a single photodetector at pulse repetition rate via space-to-time mapping technology. Wide area scanning capability is introduced by using individually addressable micro-mirror arrays as a beam deflector. Experimentally, we scanned $\sim 20 \text{ mm}^2$ at scan rate of 5 kHz with $\sim 150 \mu\text{m}$ lateral and $\sim 160 \mu\text{m}$ vertical resolution that can be controlled by using 1024×768 mirror arrays. With the current state of art MEMS technology, fast scanning with $< 30 \mu\text{s}$ and resolution down to single mirror pitch size of $10.8 \mu\text{m}$ is also achievable. [DOI: 10.1115/1.4027127]

Keywords: hybrid processes, metrology, nanomanufacturing, process control, surface treatments

1 Introduction

With the advent of micro manufacturing technology, extremely fine surface engineered solids are now reality for higher performance or for new functionalities. For instance, hydrogen fuel cells utilize bi-polar plates with microfluidic channels of dimensions as small as $5 \mu\text{m}$ at the surface to convert fuel into power via electrochemical conversion [1]. In the near future, hydrogen fuel cells are expected to become one of the main alternative energy sources and hence there will be demand for mass production of plates with micro fluidic channels, especially for automotive industry [2]. However, as the mass manufacturing of these micro textured solids becomes reality, the rapid quality control becomes a fundamental bottleneck for high yield.

Characterization of surface texture is an interest of surface metrology and it has been investigated extensively. Up to date, several techniques have been developed, mostly specialized on one aspect of the measurement at a time such as measurement of the overall shape, the small-scale features, waviness and the roughness of the surfaces [3]. In general, these various surface metrology methods are classified under three categories such as the

stylus instruments, scanning probe microscopy, and optical scanning techniques. The first technique, which is based on drawing stylus tip over the surface at constant speed, can enable up to several millimeters wide area with the detection of fine details down to $\sim 1 \mu\text{m}$ [4]. The second technique, which relies on very low contact forces between tip and surface, provides relatively highest lateral resolution ($\sim 1 \text{ nm}$) and vertical resolution down to sub nanometers, but lacks of scanning speed and limited to small scanning areas [5]. Optical scanning techniques, on the other hand, measure the surface topography by illuminating the surface through optical system and processing the reflected or transmitted light without destructive physical contact. Among these, interferometric microscopes [6] based on phase shifted interference enable monitoring of wide area with high vertical resolution ($< 0.1 \text{ nm}$) and lateral resolution close to $\sim 0.1 \mu\text{m}$. Alternatively, confocal microscopy [7], namely a focused beam version of stylus, achieves higher lateral resolution by use of a pinhole, and it is very widely used technique. Higher resolution is achievable by any of these techniques at the expense of scanning area and speed.

Fast laser scanning technology is highly desired in many applications ranging from defense to sensing and micro-manufacturing to increase the imaging speeds [8–10]. Especially, high speed ($> 1 \text{ kHz}$) scanning is essential for multi-dimensional monitoring of moving objects and to capture fast transient information of a dynamic process pertinent to light detection and ranging [11,12],

Contributed by the Manufacturing Engineering Division of ASME for publication in the JOURNAL OF MICRO- AND NANO-MANUFACTURING. Manuscript received July 11, 2013; final manuscript received February 26, 2014; published online April 8, 2014. Assoc. Editor: Liwei Lin.

structural dynamics [13,14], surface vibrometry [15], observation of biomechanical motility [16], cellular network dynamics [17], confocal and multi-photon microscopy [18,19] applications. In addition, scanning of wide area or many objects in a short period of time is also important for such high-throughput applications as atmospheric science [11], endoscopy and cytometry for medical diagnosis [20,21], geographical survey and surface profilometry in the semiconductor industry, and surface characterization and quality control in micro-manufacturing [8–10]. Various types of laser scanning techniques enabling higher scan rates have been recently proposed. Galvanometric mirrors known as the mechanically scanning mirrors are widely used for beam steering. The scanning speed of such high inertia mirrors is limited to ~ 10 kHz in 1D and ~ 100 Hz in 2D [22]. Alternatively, frequency-tunable laser in a diffractive optic bench has recently been demonstrated to achieve more than 10 times higher scanning rates [23]. In addition to the methods mentioned above, new all-optical techniques using acousto-optic deflectors (AOD) are used as a tunable diffraction grating to deflect the beam via electronically changing the angle of 1st diffraction order. Millimeter scale area imaging with $< 10 \mu\text{s}$ scanning speed and few micrometer scanning resolution has been achieved [24]. Well known real-time dispersive imaging system providing ultra fast frame rates up to tens of MHz combined with a beam deflector to enable 2D wide area scanning has been recently demonstrated [25]. However, AOD is deficient in terms of power transfer efficiency and limited deflection angles, and hence scanning area.

In this paper, we present fast dispersive laser scanning system that facilitates $\sim 20 \text{ mm}^2$ wide area scanning with $\sim 150 \mu\text{m}$ lateral and $\sim 160 \mu\text{m}$ vertical resolution at 5 kHz scanning rate by using digital micro-mirror device (DMD) technology. DMDs provide alternative fast area scanning technology that can achieve dynamic sectioning of modulated patterns via pixelated MEMS mirrors. Our proposed method using DMD technology can provide fast scanning rates up to 32.5 kHz (~ 1000 times faster than conventional scanners) and resolution down to single mirror pitch size of $10.8 \mu\text{m}$ with the state of art MEMS technology.

The DMD technology is preferred for real-time imaging, because it provides high resolution, high reflection, exceptional stability, and excellent controllability over thousands of individual micro mirrors. Also, it has already been commercialized for many applications ranging from confocal microscopy, optical networking, 3D metrology, spectroscopy to medical applications [26–28]. By spatially switching the light through micro-mirror arrays, DMD can be utilized as a digital reflective spatial light modulator. In comparison to most commonly used liquid crystal display technology, such devices provide extremely high 2D scanning speeds up to 32.5 kHz ($< 30 \mu\text{s}$ fast switching speed), higher fill factor of 90% than the liquid crystal with 70%, ~ 6.6 times higher power transfer efficiency, ~ 11 times higher contrast ratio, as twice as higher diffraction efficiency of 88% and feasibility for wide range of wavelengths (UV to near-infrared (NIR)) [29,30].

2 Experimental Setup and System Description

Figure 1 illustrates the concept of novel 2D imaging system utilizing MEMS DMD technology. Ideally large area scanning is achieved by using N pulsed lasers with the same repetition rates. Each laser will send optical impulses to image different subsection of the imaging plane. Since detection system uses single photodetector, each pulse is generated with a constant delay, $n \times \tau$, ($n = 1, 2, 3, \dots, N$), where $N \times \tau \leq T =$ repetition rate. In the proposed system, N laser array is replaced by a modelocked fiber laser as a master light source to generate broadband supercontinuum (SC) of light through nonlinear process [31]. Specifically, supercontinuum pulses are generated to provide broadband source by propagating the Mode Locked Laser pulses (at 1550 nm with < 1 ps pulse width and 20 MHz repetition rate) through a fiber-based system that consists of an amplifier (Erbium Doped Fiber Amplifier) and the cascaded single mode, dispersion shifted and

nonlinear fiber patch cords. Band pass filter (Coarse Wavelength Division Multiplexing) centered at 1590 nm is used to carve out ~ 20 nm nearly flat portion of the spectrum for scanning. In the first stage, carved SC pulses are wavelength-to-time mapped by using a dispersion compensation module (DCM with dispersion $D = -675$ ps/nm) for real-time detection. In this step, group velocity dispersion is being used to create a time delay between different colors of the pulse and hence spread spectral content linearly in time domain. The timing requirement at this stage is imposed by the overlap between lasers after time stretching. The delay between consecutive pulses (τ) should be larger than the chirped pulse width at the input of the circulator [32–34]. A pulse picking setup using optical switches follows the SC source and time wavelength mapping process to generate N parallel optical paths and to mimic the N independent lasers.

After time wavelength mapping, selected pulses are launched into free space by an array of collimators and followed by DMDs to facilitate 1D scanning. The optical pulses, on the other hand, are highly attenuated while passing through the system. The system losses are mainly due to the DCM (~ 2.1 dB insertion loss) and the DMD which induces single pass attenuation of $\sim 45\%$ by considering the beam wavelength (1590 nm), micro-mirror reflectivity ($\sim 90\%$), active area ($\sim 90\%$), diffraction efficiency (88%), and the protective cover glass on the micro mirrors (single pass transmission coefficient of $\sim 90\%$ if coated for NIR and $\sim 75\%$ if coated for visible) [14]. In the experimental setup, since power budget was not sufficient for simultaneous multichannel measurement, only one channel at a time has been used for scanning. Also, in order to compensate the system losses and to obtain a better signal-to-noise ratio (SNR), a flat gain Raman amplifier is designed to provide a uniform amplification through the DCM. The Raman amplification with ~ 10 dB net gain and < 0.5 dB gain ripple is introduced by using four pump diode lasers at wavelengths of 1450 nm, 1470 nm, 1490 nm, and 1505 nm in a hybrid pumping configuration.

In the second stage, the optical beam is expanded to illuminate the active area of the DMD, which consists of individually controllable micro-mirror arrays. Here, we use DMD mirrors fabricated by Texas Instruments. By switching the state of individual micro mirrors from ON state to OFF state, the large optical beam is digitally divided into segments and mapped to different locations at the image plane and hence beam steering is achieved as shown in Fig. 2. The spectral content of the time stretched SC pulses is dispersed by the diffractive optics which is composed of a blazed diffraction grating and a Fourier lens to illuminate each location in space by different colors of light that arrive at different times. After being mapped over the focal plane, the spectrum of the pulses is modified by the reflection and transmission property of the target image. Through the time wavelength mapping process that was achieved in fibers, the spectral modulations are mapped to the time domain at the image plane. The spectrally and temporally modulated pulses via DMD are then captured by a photo detector (> 1.2 GHz bandwidth), which is placed at the optical path that corresponds mirrors' ON state direction, while at the OFF state, beams are blocked by the setup. A real-time storage oscilloscope with 8 GHz RF bandwidth captures the electrical signals from the photodetector for post processing.

2.1 Lateral Scanning. The broadband optical pulses are spatially dispersed and focused over the space by using diffractive optics including diffraction gratings and Fourier lenses. Due to the pulse nature of the illumination, image modulation is captured by a single pulse and thus the lateral scanning rate is in megahertz, which is determined by laser repetition rate. The normalized intensity distribution $\bar{I}(x, \lambda)$, field of view (FOV) and the spatial (Δx) resolution of the pulse shaping system for both plane waves $E_p(x, d) \propto \text{rect}(x/d)$ and Gaussian waves $E_g(x, w) \propto \exp(-0.5x^2/w^2)$ where $w = d/(2\sqrt{\ln(2)})$ are calculated as

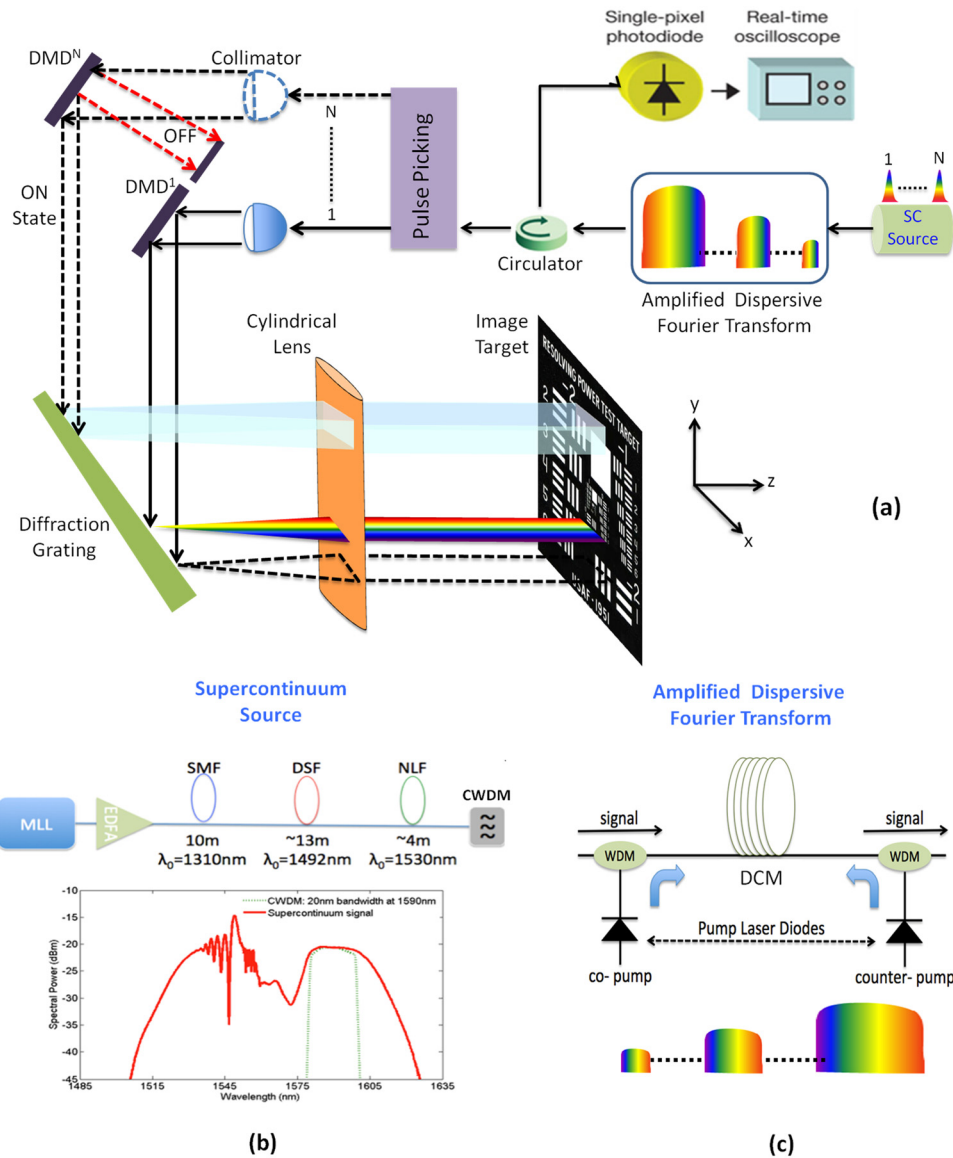


Fig. 1 The experimental setup for all optical reflective parallelized N-channel dispersive laser scanner (a). The single channel setup is used for the proof-of-concept demonstration. The supercontinuum pulse generation (b) and the amplified dispersive Fourier transform (c) modules.

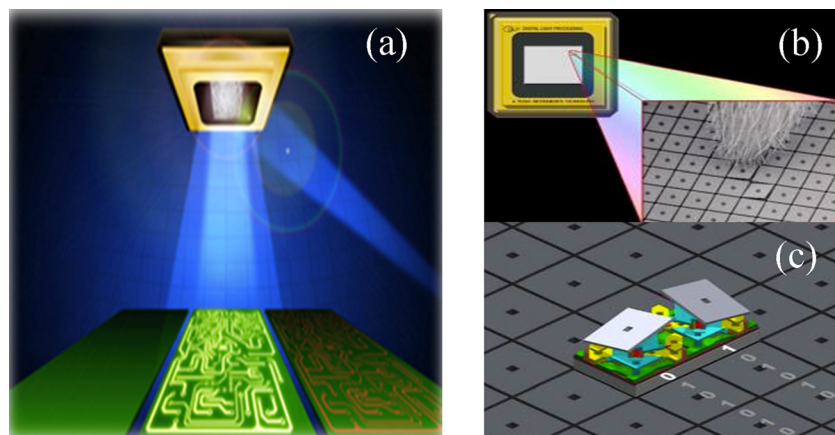


Fig. 2 DMD as a programmable beam steering technology (a) [35]. A single DMD consists of 768×1024 micro mirrors and inset shows the SEM image of micro mirrors (b). Schematics of individual micro mirrors (c) [36].

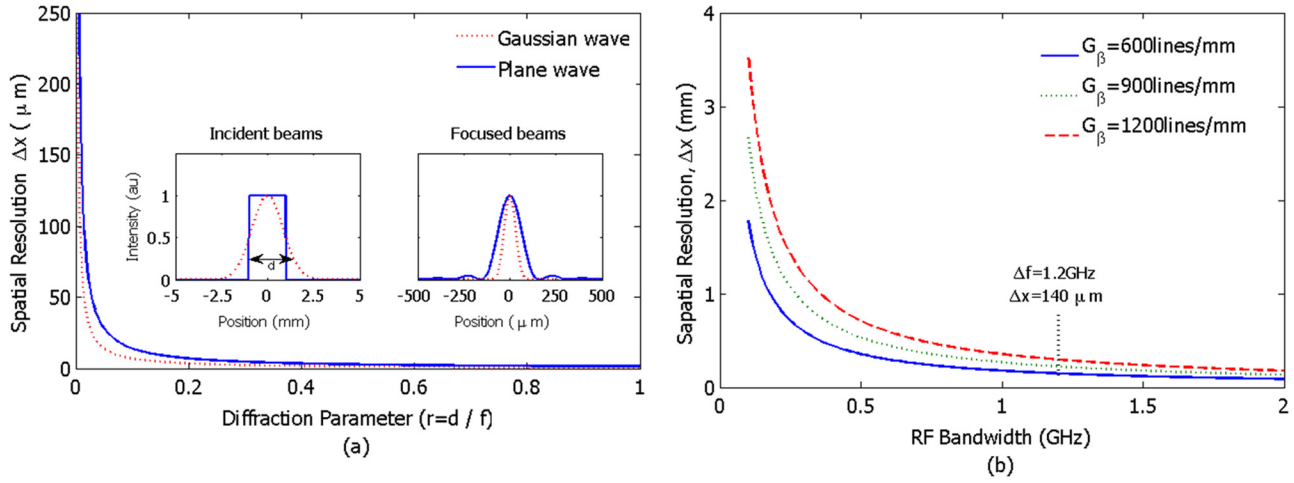


Fig. 3 The spatial resolution of the focusing system depends on the diffraction limit and is improved by increasing diffraction parameter, $r = d/f$ (a). The temporal resolution (calculated for $D = -675$ ps/nm) due to the RF bandwidth limits the spatial resolution via time-to-space mapping (b) [32].

$$\bar{I}(x, \lambda) = \begin{cases} \exp^2 \left[-\frac{\pi^2 (x - x_0)^2}{2 \ln(2) \lambda^2} \left(\frac{d}{f} \right)^2 \right], & \text{Gaussian wave} \\ \text{sinc}^2 \left[\frac{(x - x_0)}{\lambda} \left(\frac{d}{f} \right) \right], & \text{Plane wave} \end{cases} \quad (1)$$

$$\Delta x \approx \begin{cases} \frac{2\lambda f}{d\pi} \ln(2), & \text{Gaussian wave} \\ \frac{2 \times 1.39156 \lambda f}{d\pi}, & \text{Plane wave} \end{cases} \quad (2)$$

$$\text{FOV} \approx G_{\beta} f \Delta \lambda \quad (3)$$

Here f is the lens focal length, d is the beam size, $x_0 \approx G_{\beta} f (\lambda - \lambda_0)$ is the relative position of 1st order diffraction peak with respect to central wavelength (λ_0), and G_{β} is the effective groove density, which is defined as a function of 1st order diffraction angle, $G/\cos(\beta)$ [32]. The beam size is defined as the aperture size for plane waves, and full width at half maximum for Gaussian beams. The 1st order diffraction angle (β) for the incident beam at wavelength (λ) and the incident angle (α) is calculated by using the grating equation as $\sin(\alpha) + \sin(\beta) = \lambda G$ which reduces to $2 \sin(\beta) = \lambda G$ in a Littrow configuration ($\alpha = \beta$).

Final resolution of the imaging system is defined not only by the diffraction limit but also by the temporal resolution (bandwidth) of the detection system. Figure 3 illustrates the achievable resolution with respect to key parameters of optical components and the RF detection system. According to Eq. (2), the system resolution is optically limited by the diffraction limit ($r = d/f$) due to Fourier optics. By increasing the diffraction parameter ($r > 0.1$), the spatial resolution $< 10 \mu\text{m}$ is achievable, as illustrated in Fig. 3(a). In this proposed system, by changing the number of horizontal mirrors, DMD can enable tunability of the beam size and hence the diffraction limit. The lateral resolution of the system is mainly limited by the detection system. A photodetector with a given RF bandwidth (1.2 GHz used in our experiments) limits the achievable temporal resolution ($\Delta t_{\text{det}} \approx 1/\Delta f$) to ~ 800 ps which corresponds to spectral resolution ($\Delta \lambda_{\text{det}} \approx (\Delta f \cdot D)^{-1}$) of ~ 1.2 nm (due to uniform -675 ps/nm dispersion) which translates into a spatial resolution of, $\Delta x_{\text{det}} \approx (\Delta f \cdot D)^{-1} G_{\beta} f \approx 145 \mu\text{m}$, via time-to-space mapping, as illustrated in Fig. 3(b).

2.2 Vertical Scanning. In our proposed 2D imaging system, the vertical scanning is achieved by a DMD that is used as a beam

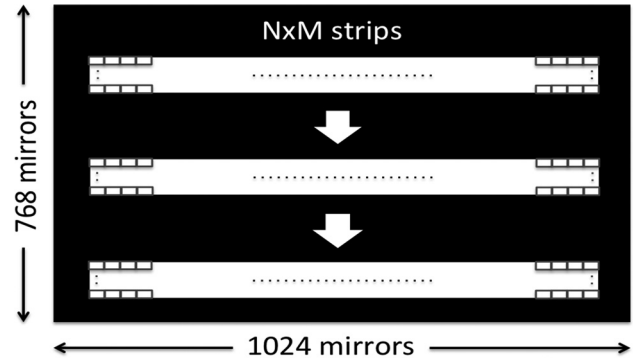


Fig. 4 The horizontal strip-type binary patterns created on DMD for laser scanning. The position of the NxM spatial mask is vertically scanned over the object by loading DMD with these dynamic patterns.

steering device. At each vertical position, SC pulses directly capture the entire lateral image by using spatio-temporal dispersive imaging technique without scanning. The lateral resolution (Δx) is determined by 4-f imaging system, which consists of diffraction grating and a Fourier lens in a double pass system, and the resolution estimated by the width of the focused beam through Eq. (2). Spatially and spectrally shaped pulses are then stretched over time by passing through the highly dispersive DCM for real-time detection.

Figure 4 illustrates the sample binary patterns created on DMD for beam steering. In these horizontal strip-type patterns, the white parts correspond to NxM arrays of ON state mirrors and the black parts correspond to OFF state mirrors. In the imaging experiment, first such horizontal strip patterns on DMD, namely narrow spatial masks, are created and then the light reflected by the mirror array is sent onto the object through a cylindrical lens. The vertical scanning is achieved by dynamically shifting this mask at the DMD, which, as a result, shifts the reflected light onto the object. Consequently, the vertical (Δy) resolution is expected to be different from what is estimated by Eq. (2). Indeed, it is determined by the number of rows of mirror arrays that switch to the same state simultaneously and the size of masks on DMD surface. Hence, a use of N rows will create an optical beam where the vertical beam waist will be $N \times 10.8 \mu\text{m}$, where $10.8 \mu\text{m}$ is the mirror pixel size at the DMD chip. Increasing the number of rows in DMD array increases the SNR, since more optical power is reflected on to the

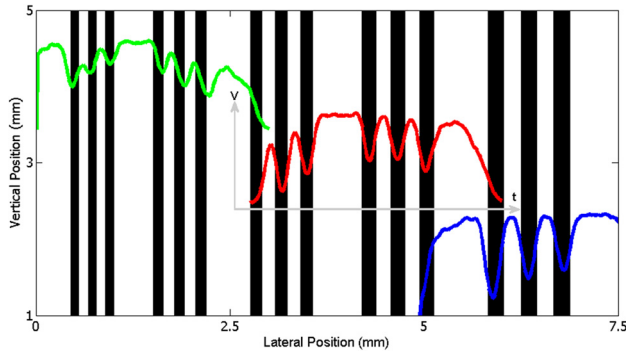


Fig. 5 The lateral resolution performance of space wavelength mapping. The vertical bars with dimensions of $\sim 150 \mu\text{m}$ to $\sim 220 \mu\text{m}$ are captured by the $\sim 13.5 \text{ ns}$ SC pulses.

object. However, it will decrease the vertical resolution, since the width of the reflected light on image increased. The vertical scanning speed is the second crucial parameter in the proposed experimental system and it is determined by the frame rate of DMD. Experimentally, DMDs with 32.5 kHz scanning speed ($\sim 30 \mu\text{s}$ switching time) can achieve ~ 600 laser pulses to illuminate the same subsection or 600 subsections for pulse picking at the same laser pulse rate (20 MHz/32.5 kHz).

3 Experimental Results

Real time imaging can work in reflection or transmission mode. To demonstrate 2D fast scanning capability, we used the time-space-wavelength mapping technique working in the reflection mode. The target image scanned by the DMD is recorded by the series of SC pulses. This 1D pulse stream (stream of horizontal line scans) with 50 ns time aperture is then segmented for different vertical coordinates, vertically aligned and digitally processed to extract the spatial features and reconstruct the original 2D image.

In this experimental study, we have used optical beam with $\sim 5 \text{ mm}$ beam size, diffraction grating with 600 lines/mm, lens with 200 mm focal length, DMD (0.55-in. diagonal mirror arrays, 1024×768 individually addressable aluminum micro mirrors, $10.8 \mu\text{m}$ pitch size, discrete states of ON (+12 deg rotation) or OFF (-12 deg rotation), and frame rate of 5 kHz) and 15×600 horizontal excitation strips to vertically scan the target image (USAF test chart) which consists of vertical black and white strips with different spatial frequencies. The proposed system can scan $\sim 20 \text{ mm}^2$ wide area ($\sim 3 \text{ mm}$ lateral ($\text{FOV}_{\text{lateral}} = G_{\text{gr}} f \Delta\lambda$) and $\sim 7.6 \text{ mm}$ vertical ($\text{FOV}_{\text{vertical}} = 768 \times 10.8 \mu\text{m}$)) with 20 MHz (pulse repetition rate) in 1D and 5 kHz (DMD frame rate) in 2D.

Figure 5 illustrates the lateral resolution performance of the dispersive imaging system. The 2D image of five groups of vertical bars with dimensions varying from $\sim 150 \mu\text{m}$ to $\sim 220 \mu\text{m}$ is captured by our dispersive laser scanner. The temporal modulation (due to spatial/spectral pulse shaping) of the SC pulses by the vertical bars with varying spatial frequencies is shown in Fig. 5. Due to the diffraction limit of the focusing system, as the spatial frequency of the patterns increases, the modulation depth decreases. Thus, we used vertically wider excitation strips ($N = 15$ mirrors) to increase the signal-to-noise ratio at the expense of diminishing vertical resolution to $\sim 160 \mu\text{m}$ compared to $10.8 \mu\text{m}$ vertical resolution that is achievable by using narrow strips of $N = 1$. In addition, vertically wider strips shifted by certain number ($n < N$) of pixels (overlapping strips) can be used to increase the SNR and to achieve higher vertical resolution ($n \times 10.8 \mu\text{m}$).

Figure 6 compares the 2D CCD image and the reconstructed images of the test target (Fig. 6(a): USAF test chart) captured by our MEMS-based dispersive laser scanner. The image is reconstructed by mapping the reflection from the target encoded on the pulse train at different scanning positions into a 2D matrix.

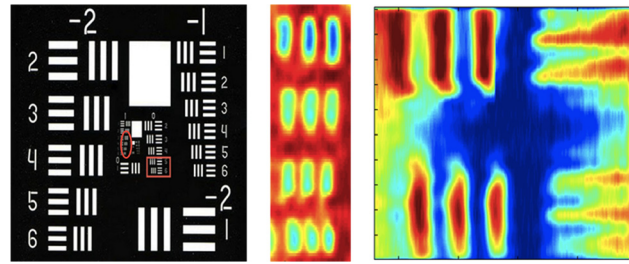


Fig. 6 Comparison between a CCD image (a) and a digitally reconstructed scan image of the target: USAF test chart Group = 1, Element 3–6 (width/line $198 \mu\text{m}$ – $140 \mu\text{m}$) (b) and Group = 0, Element 5–6 (width/line $314 \mu\text{m}$ – $280 \mu\text{m}$) (c)

Dynamically shifting the 15×600 excitation strips over the DMD at 5 kHz rate, the target is scanned with a resolution of $\sim 150 \mu\text{m}$ (lateral) and $\sim 160 \mu\text{m}$ (vertical). The captured image clearly shows the vertical and horizontal bars: Group = 1, Element 3–6 (Fig. 6(b)) and Group = 0, Element 5–6 (Fig. 6(c)).

To construct the image the normalized intensity distribution $\bar{I}(x, \lambda)$ calculated in Eq. (1) is nearly same for all the wavelengths within 20 nm spectral window centered at 1590 nm (λ_0). Thus, the intensity distribution for each wavelength is approximated as

$$\begin{aligned} \bar{I}_0(x) &\simeq \bar{I}(x, \lambda_0) \\ I(x, \lambda) &\simeq F(\lambda) \cdot \bar{I}_0(x - x_0) \end{aligned} \quad (4)$$

where $I(x, \lambda)$ is the intensity distribution and $F(\lambda)$ is the spectral power density. The space-to-wavelength mapped optical beam is both spatially and spectrally shaped by the target image $m(x)$, which can be modeled as a convolution at Fourier plane

$$y(\lambda) \simeq F(\lambda) \cdot \int \bar{I}_0(x - x_0) \cdot m(x) dx = F(\lambda) \cdot \text{conv}[I(x, \lambda), m(x)] \quad (5)$$

Spectrally encoded signals are converted into time domain

$$\left[\begin{array}{c} \text{frequency - to - time} \\ \text{mapping} \end{array} \right] \left[y(\lambda) \longrightarrow y(t) \right] \text{ via dispersive Fourier trans-}$$

formation through highly dispersive fibers. By neglecting the higher order dispersion terms, namely assuming a uniform dispersion over a wide spectrum, the temporal mapping is modeled linear as $\Delta t \simeq D \cdot \Delta\lambda$, where Δt is the temporal position of the wavelengths relative to the reference wavelength. By using such digital signal processing techniques as digital filtering and deconvolution, the spatial information of the target, $m(x)$, can be extracted.

The system performance of current experimental approach of this real-time imaging, however, is limited in terms of the spatial resolution, FOV, and the power efficiency due to following reasons. The diffraction prevents the use of bulk Fourier lenses with long focal lengths ($\propto \lambda f/d$) and hence limits the spatial resolution. Also, 1 cm^2 active area of the DMD combined with diffraction gratings ($\sim 3.5 \text{ deg}/100 \text{ nm}$ spatial dispersion with 600 lines/mm groove density) limits the field of view. Finally, high losses due to higher order diffractions limit the power efficiency of the system. In order to achieve resolution close to $20 \mu\text{m}$ and lower, the system should be able to illuminate the whole imaging sample with frequency-time and space-time mapped light, focus the light everywhere on the sample to $< 20 \mu\text{m}$ spot size and should be low loss for high contrast imaging. Furthermore, in order to make the system compatible with manufacturing technology the working distance should be long, $> 0.5 \text{ mm}$ to avoid contact and contamination. Planar optical devices such as lenses or diffraction

optics combined with real time imaging can facilitate high-resolution imaging in real time.

4 Conclusion

We have proposed a fast dispersive laser scanning system by using MEMS micro-mirror technology. Two-dimensional beam steering is employed by combining the space wavelength mapping for the lateral scanning and digital micro-mirror arrays for vertical scanning. By dynamically switching the states of the micro mirrors, the position of the spatially dispersed beam is moved over the target. We have monitored $\sim 20 \text{ mm}^2$ wide area with $\sim 150 \mu\text{m}$ lateral and $\sim 160 \mu\text{m}$ vertical resolution for the proof of concept. We estimate that MEMS-based amplified time stretched system can achieve fast vertical scanning with frame rates up to 32.5 kHz and with resolution down to single mirror pitch size of $10.8 \mu\text{m}$.

References

- [1] Etch, T., 2010, "Photoetched Fuel Cell Plates, Frames, Support Screens & End Caps," <http://www.tech-etich.com/photoetch/fuelcell.html>
- [2] IPHE, 2010, "The Role of Battery Electric Vehicles, Plug-in Hybrids and Fuel Cell Electric Vehicles," http://www.iphe.net/docs/Resources/Power_trains_for_Europe.pdf
- [3] Wilkening, G., and Bosse, H., 2005, "Nano- and Micrometrology State-of-the-Art and Future Challenges," MAPAN-J. Metrol. Soc. India, **20**(2), pp. 125–151.
- [4] Hansen, H. N., Tosello, G., Gasparin, S., and De Chiffre, L., 2011, "Dimensional Metrology for Process and Part Quality Control in Micro Manufacturing," *Int. J. Precis. Technol.*, **2**(2–3), pp. 118–135.
- [5] Danzebrink, H. U., Koenders, L., Wilkening, G., Yacoot, A., and Kunzmann, H., 2006, "Advances in Scanning Force Microscopy for Dimensional Metrology," *Cirp Ann.-Manuf. Technol.*, **55**(2), pp. 841–878.
- [6] Wyant, J. C., 1974, "White-Light Extended Source Shearing Interferometer," *Appl. Opt.*, **13**(1), pp. 200–202.
- [7] Minsky, M., 1988, "Memoir on Inventing the Confocal Scanning Microscope," *Scanning*, **10**(4), pp. 128–138.
- [8] Marshall, G. F., and Stutz, G. E., 2004, *Handbook of Optical and Laser Scanning*, Taylor & Francis, Boca Raton, FL.
- [9] Fujii, T., and Fukuchi, T., 2005, *Laser Remote Sensing*, Taylor & Francis, Boca Raton, FL.
- [10] Dotson, C., Harlow, R., and Thompson, R. L., 2003, *Fundamentals of Dimensional Metrology*, Thomson Learning, Albany, NY.
- [11] Weitkamp, C., 2005, *Lidar: Range-Resolved Optical Remote Sensing of the Atmosphere*, Springer, Berlin, Germany.
- [12] Schwarz, B., 2010, "LIDAR: Mapping the World in 3D," *Nat. Photonics*, **4**(7), pp. 429–430.
- [13] Sinha, A., 2010, *Vibration of Mechanical Systems*, Cambridge University Press, New York.
- [14] Osten, W., 2006, *Optical Inspection of Microsystems*, Taylor & Francis, Boca Raton, FL.
- [15] Pelesko, J. A., and Bernstein, D. H., 2002, *Modeling MEMS and NEMS*, Taylor & Francis, Boca Raton, FL.
- [16] Popescu, G., Ikeda, T., Goda, K., Best-Popescu, C. A., Laposata, M., Manley, S., Dasari, R. R., Badizadegan, K., and Feld, M. S., 2006, "Optical Measurement of Cell Membrane Tension," *Phys. Rev. Lett.*, **97**(21), p. 218101.
- [17] Goebel, W., Kampa, B. M., and Helmchen, F., 2007, "Imaging Cellular Network Dynamics in Three Dimensions Using Fast 3D Laser Scanning," *Nat. Methods*, **4**(1), pp. 73–79.
- [18] Pawley, J. B., 1995, *Handbook of Biological Confocal Microscopy*, Plenum Press, New York.
- [19] Denk, W., Strickler, J. H., and Webb, W. W., 1990, "2-Photon Laser Scanning Fluorescence Microscopy," *Science*, **248**(4951), pp. 73–76.
- [20] Hoffman, A., Goetz, M., Vieth, M., Galle, P. R., Neurath, M. R., and Kiesslich, R., 2006, "Confocal Laser Endomicroscopy: Technical Status And Current Indications," *Endoscopy*, **38**(12), pp. 1275–1283.
- [21] Tarnok, A., and Gerstner, A. O. H., 2002, "Clinical Applications of Laser Scanning Cytometry," *Cytometry*, **50**(3), pp. 133–143.
- [22] Conant, R., 2002, *Micromachined Mirrors*, Vol. 12, Springer, New York.
- [23] Yaqoob, Z., and Riza, N. A., 2004, "Passive Optics No-Moving-Parts Barcode Scanners," *IEEE Photonics Technol. Lett.*, **16**(3), pp. 954–956.
- [24] Goutzoulis, A. P., Pape, D. R., and Kulakov, S. V., 1994, *Design and Fabrication of Acousto-Optic Devices*, M. Dekker, New York.
- [25] Goda, K., Mahjoubfar, A., Wang, C., Fard, A., Adam, J., Gossett, D. R., Ayazi, A., Sollier, E., Malik, O., Chen, E., Liu, Y., Brown, R., Sarkhosh, N., Di Carlo, D., Jalali, B., 2012, "Hybrid Dispersion Laser Scanner," *Sci. Rep.*, **2**.
- [26] Jung, I. W., Wang, J. S., and Solgaard, O., 2007, "Optical Pattern Generation Using a Spatial Light Modulator for Maskless Lithography," *IEEE J. Sel. Top. Quantum Electron.*, **13**(2), pp. 147–154.
- [27] Dudley, D., Duncan, W. M., and Slaughter, J., 2003, "Emerging Digital Micromirror Device (DMD) Applications," *Proc. SPIE*, **4985**, pp. 14–25.
- [28] Nayar, S. K., Branzoi, V., and Boulton, T. E., 2004, "Programmable Imaging Using a Digital Micromirror Array," Proceedings of the 2004 IEEE Computer Society Conference on Computer Vision and Pattern Recognition, Vol. 1, pp. I-436–I-443.
- [29] DLP Texas Instruments, 2010, "DLP 0.55XGA Chipset," <http://www.ti.com/lit/ml/dlpb003/dlpb003.pdf>
- [30] Nesbitt, R. S., Smith, S. L., Molnar, R. A., Benton, S. A., 1999, "Holographic Recording Using a Digital Micromirror Device," *Proc. SPIE*, **3637**, pp. 12–20.
- [31] Boyraz, O., Kim, J., Islam, M. N., and Jalali, B., 2000, "10 Gb/s Multiple Wavelength, Coherent Short Pulse Source Based on Spectral Carving of Supercontinuum Generated in Fibers," *J. Lightwave Technol.*, **18**(12), pp. 2167–2175.
- [32] Kalyoncu, S. K., Huang, Y., Song, Q., and Boyraz, O., 2012, "Analytical Study on Arbitrary Waveform Generation by MEMS Micro Mirror Arrays," *Opt. Express*, **20**(25), pp. 27542–27553.
- [33] Kalyoncu, S. K., Huang, Y., Song, Q., and Boyraz, O., 2013, "Fast Arbitrary Waveform Generation by Using Digital Micromirror Arrays," *IEEE Photonics J.*, **5**(1), pp. 302–303.
- [34] Kalyoncu, S. K., Huang, Y., Torun, R., Zhao, Q., and Boyraz, O., 2013, "Fast Dispersive Laser Scanner by Using Digital Micro Mirror Arrays," CLEO Conference 2013, San Jose, CA.
- [35] DLP Texas Instruments, 2010, "Digital Exposure," <http://www.ti.com/analog/docs/memsmidlevel.tsp?sectionId=622&tabId=2455>
- [36] GNT, "Presentation of the DLP Technology," <http://us.generation-nt.com/technology-dlp-video-projector-digital-light-processing-review-42606-2.html>